Journal of Metals, Materials and Minerals, 34(1), 1926, 2024

Microstructural and dielectric characteristics of the Ce-doped Bi_2FeMnO_6

Laxmidhar SAHOO[1], Swayam Aryam BEHERA[1], Rajesh Kumar SINGH[2], Santosh Kumar PARIDA[3,*], and Patnala Ganga Raju ACHARY[1,*]

[1] *Department of Chemistry, ITER, Siksha 'O' Anusandhan Deemed to be University, Bhubaneswar, 751030, India*
[2] *Department of Chemistry, Maharaja Sriram Chandra Bhanja Deo University, Takatpur, Baripada-757003, Odisha, India*
[3] *Department of Physics, ITER, Siksha 'O' Anusandhan Deemed to be University, Bhubaneswar, 751030, India*

***Corresponding author e-mail**: pgrachary@soa.ac.in, santoshparida@soa.ac.in

Received date:
30 December 2023
Revised date
11 January 2024
Accepted date:
6 February 2024

Keywords:
$Bi_2FeMn_{0.94}Ce_{0.06}O_6$;
Double perovskite;
Dielectrics;
Loss tangent

Abstract

A double-perovskite material $Bi_2FeMn_{0.94}Ce_{0.06}O_6$ (BFMCO) was synthesized by solid state reaction technique and characterized it by various techniques (structural, microstructural, dielectric, impedance and modulus properties). The material has an orthorhombic crystal structure with an average crystallite size of 52.4 nm, as revealed by X-ray diffraction data (XRD). The scanning electron microscope (SEM) image shows the presence of nano rod-shaped grains and well-defined grain boundaries in this material, with an average grain size of 21.8 µm. The Energy dispersive X-ray (EDX) analysis and color mapping confirm the purity and the composition of the material. The dielectric, impedance and modulus properties are investigated in the temperature range of 25°C to 500°C and frequency range of 1 kHz to 1 MHz. The material exhibits a high dielectric constant at low frequency region and a low dielectric loss, which make it a suitable candidate for better energy storage devices. The impedance study reveals the negative temperature coefficient of resistance (NTCR) behavior of the material. The modulus study indicates the non-Debye relaxation of the material. The semi-conducting nature of the material is verified by the semi-circular arcs observed in both Nyquist and Cole-Cole plots. Thermally activated conduction mechanism is confirmed from ac conductivity study.

1. Introduction

Multiferroic materials have been the main subject of extensive research over the past few decades. They have grown to be a significant components of the industries owing to their amazing prospective in multifunctional applications including magneto-electric sensor like devices, transducers, filters, and electromechanical devices like spintronics. Perovskites are special type of materials with ABO_3 like structure which exhibit remarkable properties and hence paying attention to the researchers in the last few years [1-4]. The multiferroics are mostly shown by perovskite materials and the wide range of electrical characteristics offered by perovskite materials includes metallic, ferroelectric-antiferroelectric and semiconducting nature. Ferroelectric materials may be one of the categories of pyro electric, piezoelectric, and ferro elastic and extend the application ranges in various dimensions of science and technological fields like electrical devices, capacitors, etc. and extremely useful for the manufacturing of sensors, infrared detectors, optical switches, filters, actuators etc. [5-7]. In last few years, Double perovskites have also made too much interest to the researchers owing to their high curie temperature and half metallicity and for which they can function as a ferrimagnetic insulators. The magnetic characteristics of double perovskites can be governed by exchange mechanism of B and B′ site via an oxygen atom. For multiferroicity [8,9], energy applications [10], solar cells [11,12], and other uses, double perovskites such as Sr_2FeMoO_6 and Bi_2FeMoO_6 (and other blending of acceptable substitutions for cations and anions) are utilized. In this regard, we investigated double perovskites for usage as the electrodes in magnetic tunnel junctions (MTJs), such as Bi_2FeMoO_6, La_2MnNiO_6, and Bi_2MnMoO_6 [13,14]. We keep finding new materials of multiferroicity at room temperature, materials having high spin polarization and high Curie temperatures for spintronics devices. Thus, Bi_2FeMnO_6 is more appropriate double perovskite which has been the subject of research [15-18], and among these papers, majority reported papers are based on thin films, which are crystalize in R3c symmetrical structure. The magnetic behavior of the material, Bi_2FeMnO_6 can be described by the help of spin frustration model [19]. Furthermore, Double perovskites may be a better alternative compared to single perovskites because of their bigger capacity to accommodate the extra atoms, complex structure with enhanced physical properties, improved chemical stability, and better potential applications [20]. Increased oxygen vacancies in double perovskites may affect the conductivity, which is good for electrochemical performance [21]. The dopants and synthesis processes affect the unusual physical properties of the double perovskites.The improved dielectric properties and transport mechanism in the double perovskite may be suitable for multilayer capacitors, memory, and microelectronic devices [22-24]. In this connection, we have gone through the journal article of cerium doped $NiFe_2O_4$ ferrite which fabricated by solid state

reaction technique and this material was reported by Shirsath *et al.* (2011). They explained that the pore mobility in $NiFe_2O_4$ ferrite was enhanced by doping of Ce^{4+} ion and for which excess cation vacancies was generated that affect bulk density and overall grain growth, for which material becomes important in connection to the application [25]. There are some lead-free ceramic compounds having various applications in sensor related devices [26-29].

Although there are many research articles related to the Bi_2FeMnO_6 samples, the study on low-concentration cerium doped Bi_2FeMnO_6 material is scared in the literature. Therefore, it was decided by the authors to explore some novel physical properties of the cerium-modified Bi_2FeMnO_6 at low concentrations. In this regard, we describe the synthesis and characterisation of a novel double perovskite material, $Bi_2FeMn_{0.94}Ce_{0.06}O_6$. Additionally, it was stated in this paper that cerium ion doping into Bi_2FeMnO_6 on Mn site is a reliable way to stabilise the growth of orthorhombic crystal structure and also modify its physical properties. Moreover, we report the surface morphology, dielectric, impedance and modulus properties of the proposed compound $Bi_2FeMn_{0.94}Ce_{0.06}O_6$ which will be described in more detail in the next section along with searching some suitable device applications.

2. Experimental method

Bi_2O_3, MnO_2, CeO_2 and $FeCO_3$ of Loba Chemical Pvt. Ltd. with more than 99% purity were taken in an agate mortar and pestle mixed well to get fine powder. About 50 mL methanol were added to this powdered sample and grinded for 2 h to get homogeneous mixture and then transferred to an alumina crucible. The crucible was put in a temperature programmed furnace at 1100°C for 10 h used for calcination at the rate of $2°C \cdot min^{-1}$. By using XRD (RIGAKU Japan ULTIMA IV) pattern, the phase formation of the calcined sample was verified. Polyvinyl alcohol (PVA) binder was mixed with some quantities of calcined powdered sample and got two circular pellets having diameter 10 mm and thickness 1 mm by using KBr hydraulic press with axial pressure of 4×10^6 $N \cdot m^{-2}$. Then the pellets were sintered at 1150°C and got moisture free, more condensed and homogeneous distribution of particles in the studied material. The chemical equation for the proposed material can be written as;

$$Bi_2O_3 + FeCO_3 + 0.94MnO_2 + 0.06CeO_2 \rightarrow Bi_2FeMn_{0.94}Ce_{0.06}O_6 + CO_2 \uparrow$$

3. Results and discussion

3.1 Formation of sample

Tolerance factor is a significant factor to confirm the stability of a perovskite (ABO_3) material and it is known from the Equation, $t = r_A + r_o/\sqrt{2}(r_B + r_0)$ at where r_A = ionic radius of atom A, r_B = ionic radius of atom B, and r_0 = ionic radius of oxygen atom [30]. However, the modified relation for our synthesized double perovskite can be written as;, $t = \frac{R_{A'+A''}}{2} + R_O/\sqrt{2}(\frac{R_{B'+B''}}{2} + R_O)$ where $R_{A'}$, $R_{A''}$, $R_{B'}$, $R_{B''}$, and R_O are the ionic radii of Bi, Fe, Mn, Ce, and O respectively [31-33]. The tolerance factor of the studied material was calculated as 0.84 that approves a stable double perovskite formation in an orthorhombic crystal structure.

3.2 XRD study

XRD method helps to recognize unidentified structure, unit cell, space group, density and volume of a material. Figure 1 indicates the XRD pattern of calcined and powdered BFMCO ceramic material.

A single-phase orthorhombic structure appears to have formed, according to the preliminary structural study. The POWDMULT software is employed to determine the crystal structure and lattice parameters [34] of this material. Orthorhombic crystal structure is predicted by structural analysis when the computed and experimental (observed) inter-planner distances agree as much as possible with the least amount of standard deviation. Using the orthorhombic crystal structure, POWDMULTs software indexes all the prominent XRD peaks. The evaluated cell parameters of the studied material are $a = 12.6316$Å, $b = 8.8927$ Å, $c = 7.2586$ Å having $\alpha = \beta = \gamma = 90°$ and $V = 815.64$ $Å^3$. The crystalline nature of the prepared sample is shown by the peak's clarity and sharpness [35]. The orthorhombic crystal symmetry of this material is used for investigating structural properties. By using Scherer's formula; $D = k\lambda/\beta cos\theta$, the average crystallite size of the BFMCO ceramic was calculated and where β = full-width half maximum in radian, k = anisotropic constant (~ 0.89), D = average crystallite size, λ = wave length (1.54 Å) and θ = peak position [36]. The value of average crystallite size of this material is 52.4 nm which was calculated by using one of the higher intense diffraction peak at 32.58° as a reference.

3.3 SEM and EDX study

The distribution and growth of grain which affect the conduction mechanism of the sample can be explained from Scanning electron microscope (SEM) analysis. Figure 2(a) represents the surface micro-structure (SEM micrograph), (b) EDX spectrum, (c) color mapping and (d) Gaussian fitted grain size of the $Bi_2FeMn_{0.94}Ce_{0.06}O_6$ ceramic at room temperature.

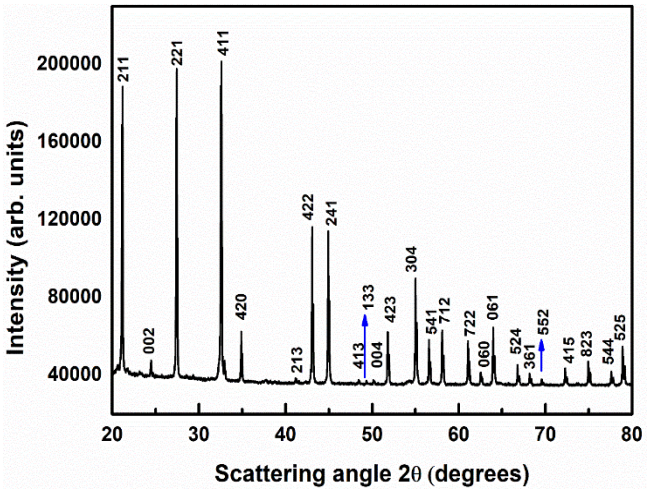

Figure 1. XRD pattern analysis of BFMCO material

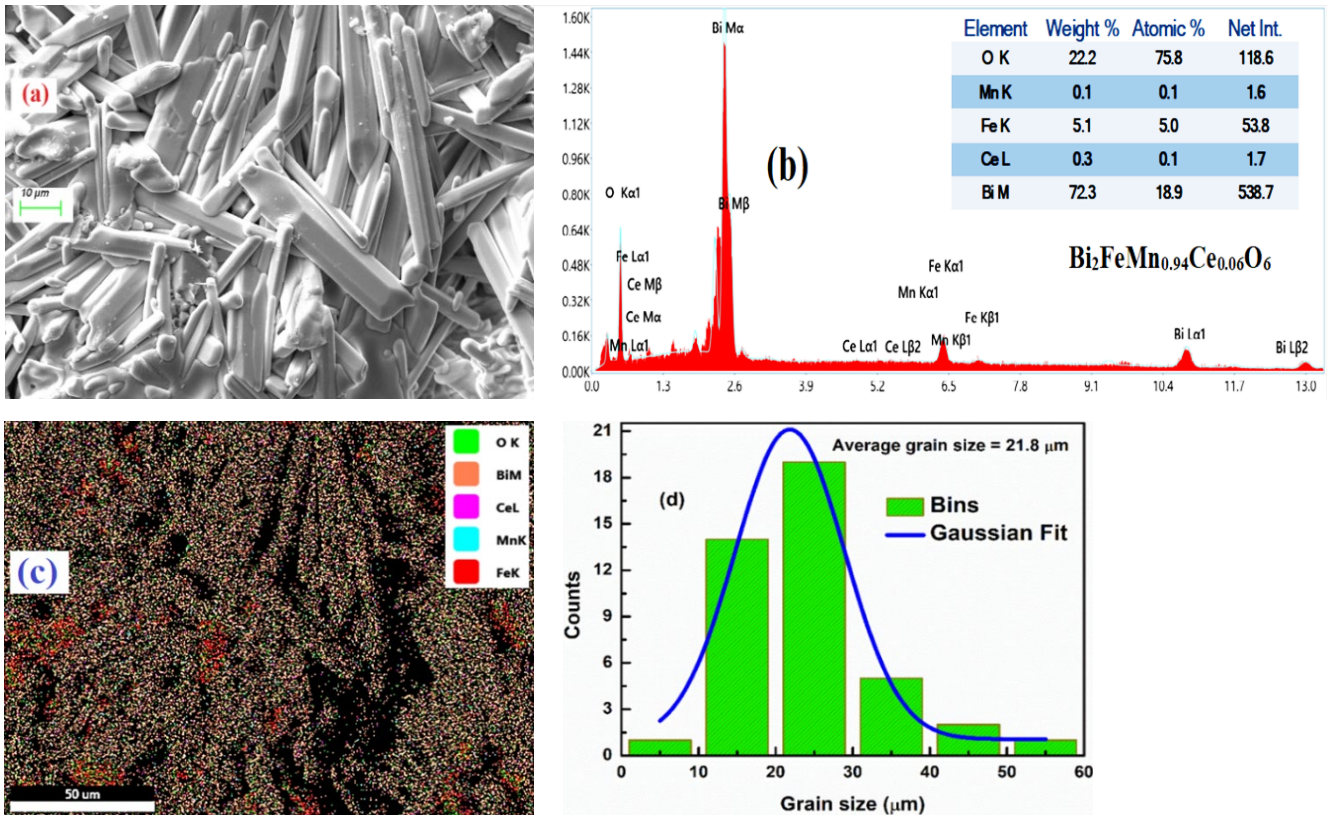

Figure 2. (a) SEM micrograph, (b) EDX spectrum, (c) color mapping, and (d) Gaussian fitted grain size of the BFMCO ceramic.

The SEM micrograph examination reveals elongated Nano rod-type grains that are uniformly dispersed across the surface of the prepared material with well-defined grain boundaries. The presence of insignificant voids is indicated by the compactness of the grains through distinct grain borders. The existence of all the constituent elements (Bi, Fe, Mn, Ce, and O) in the analyzed material is confirmed from energy dispersive X-ray (EDX) analysis which contains all the components inside the material both in exact weight and atomic percentage. The color mapping of the studied sample shows the presence of all constituent elements and distribution of the elements over the sample surface is uniform. The average grain size of this material is 21.8 µm which is calculated using Image J software.

3.4 Dielectric study

Relative dielectric permittivity can be used to determine a material's ability to store electrical energy from an applied electric field which is calculated by dividing the field strength in a material medium by the field strength in a vacuum media. When an electric field is given to a material, the charges within it causing the atoms and molecules to vibrate and for which the charged ions are forced from their equilibrium site to increase polarization. The change of dielectric constant and tangent loss with frequency are known from real and imaginary parts of dielectric permittivity and the related Debye formula is given as $\varepsilon' = \varepsilon_\infty + (\varepsilon_s - \varepsilon_\infty)/1 + \omega^2\tau^2$, $\varepsilon'' = \varepsilon_\infty + (\varepsilon_s - \varepsilon_\infty)\omega\tau/1 + \omega^2\tau^2$, and $\tan\delta = \varepsilon''(\varepsilon_s - \varepsilon_\infty)\omega\tau/\varepsilon'\varepsilon_s + \varepsilon_\infty\omega^2\tau^2$, where ε_s is denoted as static dielectric constant and ε_∞ is denoted as dielectric constant at very high frequency, ω is the angular frequency and τ is the relaxation time. The dielectric properties of the perovskite materials can be studied from the change of dielectric constant and tangent loss with both frequency and temperature. The dielectric constant can be found out by using the formula; $\varepsilon_r = C_p/C_0$, and $C_0 = \varepsilon_0 A/t$, where ε_0 = the relative permittivity of the medium = 8.85×10^{-12} F·m^{-1}, t = thickness of the pellet and A = area of cross-section of the pellet. It is well known that dielectric properties depend upon the polarization process in the materials after the application of an external ac electric field.

Figure 3(a) depicts the change of frequency versus dielectric constant at various temperatures ranging from 25°C to 500°C and from this figure it is observed that dielectric dispersion is high at low frequency zone due to accumulation of space charge carriers at the interface of grain boundaries and then reduces as frequency increase. It was explained by Maxwell-Wagner polarization theory [37]. According to this theory, there are four types of polarizations namely electronic, dipolar, ionic, and space charge polarization are existed in the sample, but the influence of the space charge polarizations are more dominance at low frequency zone. Again, on account of decrease in space charge polarization, dielectric constant values decrease when frequency increases [38]. Furthermore, the steep slope appearance which is quite steep at a low-frequency region on account of grain boundary effect, and shallow slope appearance at high-frequency zone due to grain effect are shown in Figure 3 (a) [39]. Interestingly, Koop's two-layer model theory can also describe the high dielectric dispersion nature of of this material.

The change of frequency against tangent loss at various temperatures ranging from 25°C to 500°C is depicted in Figure 3(b). From this graph it is observed that there is wide dispersion of dielectric loss (tan δ) at low frequency zone which is due to misalignment of electric dipoles. Such type of dispersion nature of both dielectric constant and dielectric loss at low frequency zone can be explained by the Maxwell-Wagner polarization effect. On the basis of such theory, the dielectric medium support strongly by conducting grains sensitive near high frequency and resistive grain boundaries sensitive near low frequency. At low frequencies, mobile ions between Fe^{2+}/Fe^{3+} hop at their respective octahedral locations, but at high frequencies, this hopping process is suppressed owing to the quick changing of the supplied external ac field [40]. Thus, Electrons are able to move through conducting grains and weak conducting grain borders on account of this hopping process.

The information regarding the dielectric properties of the studied BFMCO ceramic at specific frequency range (1 kHz to 1 MHz) are given in Figure 3(c-d) which also represent the change in temperature against dielectric constant and dielectric loss (tan δ). It is observed from these two figures that both dielectric constant and tangent loss have low value at low temperature region which is due to inert character of ions, passiveness of mobile electrons and polarons. Moreover, at low temperatures, charge carriers are less thermally activated and less mobile, leading to a lower dielectric response. However, the dielectric constant increases at high temperatures owing to the presence of space charge polarization, electronic dispersal between Fe^{2+} and Fe^{3+} ions, thermally active mobile charge carriers and activation of electron hopping. The value of dielectric loss also increases at high temperature region and it is due to increase in vibrations of ferrite ions at the octahedral site and also presence of defects. These factors contribute to enhanced polarization and charge movement in the material, resulting in a higher dielectric response [41]. In good dielectric materials, the dielectric loss decreases at higher frequencies, indicating that charge carriers can follow the alternating electric field more effectively, resulting in lower energy losses [42].

Overall, the dielectric studies in Figure 3(a-d) reveal important characteristics of the studied sample. The rise in dielectric properties with increase in temperature is attributed to the presence of space charge polarization and thermally active charge carriers. The low dielectric loss and its frequency behavior indicate that the material has good dielectric properties and hence will make it a good material for several applications where efficient energy storage and low energy dissipation are essential. These findings contribute to this material for understanding the electrical behavior and its possible applications in electronic and capacitor devices.

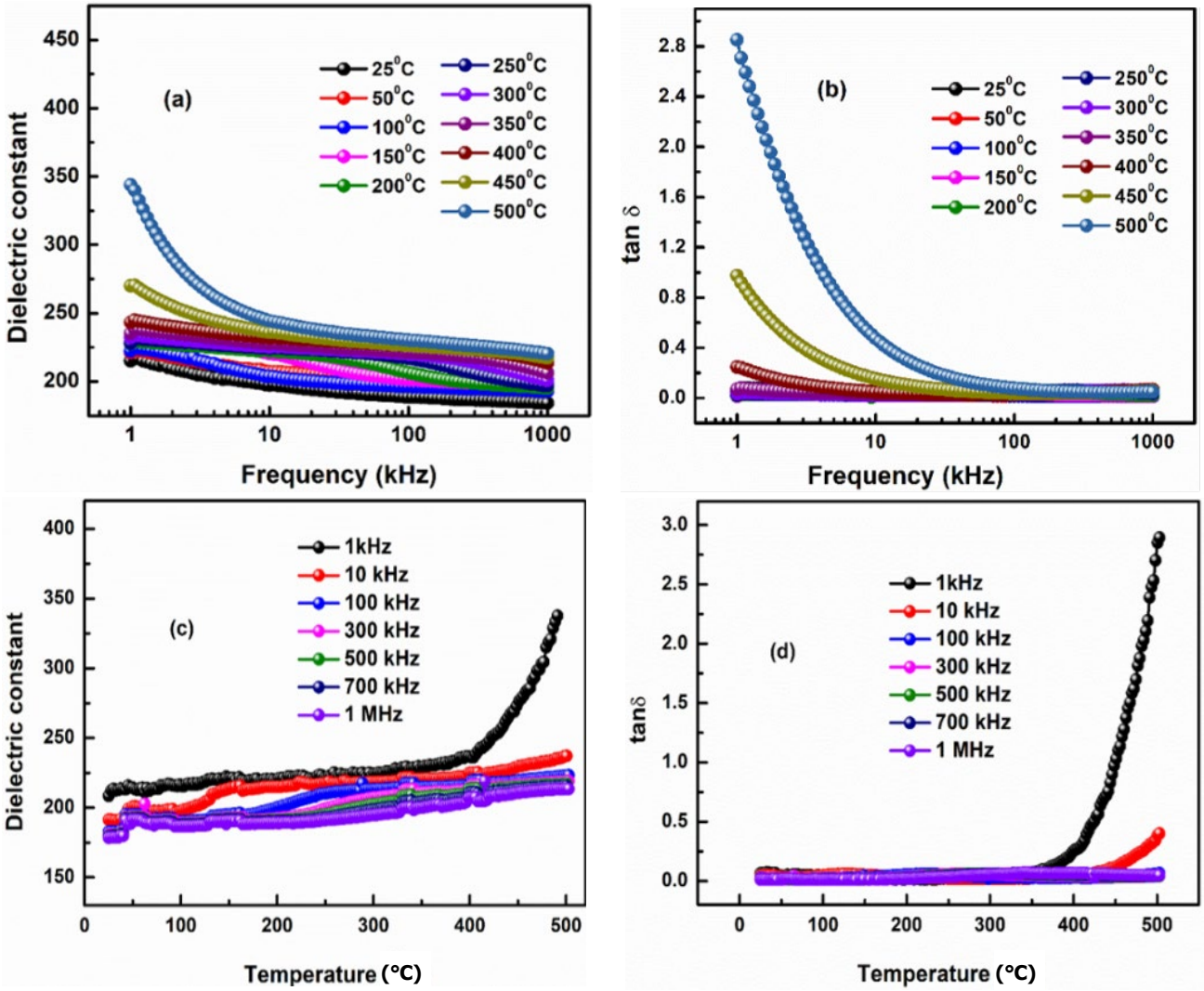

Figure 3. (a) Frequency vs. Dielectric constant, (b) Frequency vs. tanδ, (c) Temperature vs. Dielectric constant, and (d) Temperature vs. tan δ of the BFMCO ceramic.

3.5 Impedance study

The relationship between the electrical and microstructural properties of a material is revealed through impedance analysis. This technique explains the electrical properties of the material with regard to quality of the material or ceramic formation, bulk (grain), grain boundaries, transport qualities and charge storage capacity. The frequency against real and imaginary impedance (Z′ and Z″) at various chosen temperatures (25°C to 500°C) is shown in Figure 4(a-b). The interpretation of these impedance components provides valuable understandings to the electrical behaviour and properties of the material under investigation. It is observed from the Figure 4(a) that the value of Z′ decreases at the low-frequency region when temperatures increase. This behaviour is the characteristics of negative temperature coefficient resistance (NTCR) [43]. It is a well-known fact that the resistance decreases with the increase in temperature in NTCR materials, which usually observed in certain semiconductors [44]. This behaviour is significant for applications where temperature sensing or temperature compensation is required. At high frequencies (above 10 kHz), the Z′ values completely merge irrespective of temperatures supporting the semiconducting nature, and also the release of interfacial charges contribute to this behaviour [45-46]. The imaginary component of impedance (Z″) adopts same fashion to Z′, as described in Figure 4(b). The behaviour of Z″ also supports the NTCR behaviour at low frequencies and the semi-conducting properties at high frequencies, as discussed for Z′. Figure 4(c) shows Nyquist's plots at specific selected temperatures (25°C to 500°C) and from this figure semi-circular arcs are observed which is a supporting feature of the semiconducting nature of the studied sample [47]. Figure 4(d) shows the fitted Nyquist plots at some selected temperatures. It is observed that all the data points are well fitted with ZSIMPWIN software 2.0 version and found that resistance decreases with rise of temperature. So, it is also strongly support NTCR nature of the studied sample.

Overall, the analysis of impedance components (Z′ and Z″) provide important information about the electrical properties of the material at different temperatures and frequencies. The observed NTCR behaviour and the semiconducting properties have implications for potential applications of the material in temperature sensors, electronic devices, and other technologies that rely on electrical properties. These findings are very important for understanding the electrical properties of the studied double perovskite compound and its prospective applications in electronic devices and sensors.

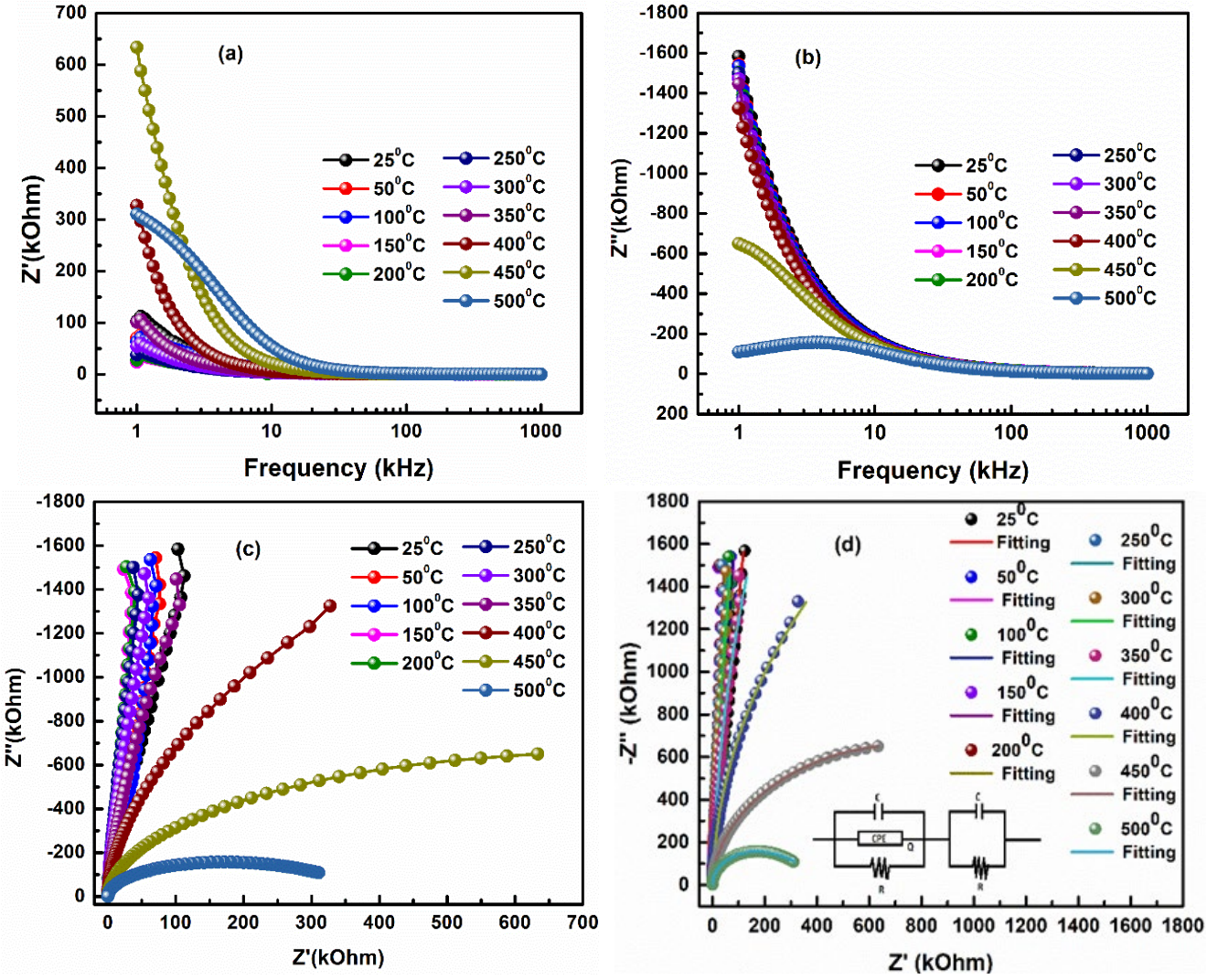

Figure 4. (a) Frequency vs. real impedance (Z′), (b) Frequency vs. imaginary impedance (Z″), (c) Nyquist plots and (d) fitted Nyquist plots at specific temperatures of the BFMCO ceramic

Table 1. Fitting parameters.

Temp (°C)	C_b ($F \cdot cm^{-2}$)	Q ($S\text{-}s^5 \cdot cm^{-2}$)	R_b ($\Omega\text{-}cm^2$)	n	C_{gb} ($F \cdot cm^{-2}$)	R_{gb} ($\Omega\text{-}cm^2$)
25	3.514E–010 Expt.)	7.149E–009(Expt.)	3.054E+005(Expt.)	1.77	1.095E–010(Expt.)	2.118E+007(Expt.)
	3.514E–010 (Fitting)	7.148E–009 (Fitting)	3.055E+005(Fitting)		1.095E–10(Fitting)	2.119E+008(Fitting)
50	9.983E–012(Expt.)	2.322E–009(Expt.)	6.647E+004(Expt.)	1.56	1.058E–010(Expt.)	7.249E+007(Expt.)
	9.972E–012(Fitting)	2.322E–009(Fitting)	6.644E+004(Fitting)		1.058E–010(Fitting)	7.241E+007(Fitting)
100	3.569E–010(Expt.)	1.473E–007(Expt.)	5.327E+004(Expt.)	2.32	1.056E–010(Expt.)	7.905E+007 (Expt.)
	3.567E–010(Fitting)	1.473E–009(Fitting)	5.327E+004(Fitting)		1.056E–010(Fitting)	7.903E+007(Fitting)
150	2.574E–019(Expt.)	1.407E–009(Expt.)	1.069E+004(Expt.)	90.90	1.067E–010(Expt.)	6.291E+007(Expt.)
	2.569E–019(Fitting)	1.405E–009(Fitting)	1.069E+004(Fitting)		1.068E–010(Fitting)	6.272E+007(Fitting)
200	5.891E–010(Expt.)	1.354E–005(Expt.)	7.069E+007(Expt.)	362.00	1.062E-010(Expt.)	5.078E+006(Expt.)
	5.892E–010 (Fitting)	1.353E–005(Fitting)	5.202E+007(Fitting)		1.062E–010(Fitting)	5.086E+007(Fitting)
250	4.828E–010(Expt.)	6.994E–007(Expt.)	1.316E+013(Expt.)	28.30	1.064E–010 (Expt.)	3.908E+007(Expt.)
	4.828E–010 (Fitting)	6.994E–006(Fitting)	1.435E+013(Fitting)		1.064E–010(Fitting)	3.908E+007(Fitting)
300	9.952E–011(Expt.)	7.176E–012(Expt.)	9.943E+007 (Expt.)	2.15	8.702E–010(Expt.)	2.855E+002(Expt.)
	9.952E–011 (Fitting)	7.174E–011(Fitting)	9.938E+007(Fitting)		8.702E–010(Fitting)	2.855E+002 (Fitting)
350	1.000E–025 (Expt.)	4.378E–008(Expt.)	3.744E+004 (Expt.)	6.40	1.108E–010(Expt.)	1.826E+007(Expt.)
	1.000E–025(Fitting)	4.378E–008(Fitting)	3.744E+004(Fitting)		1.108E–010(Fitting)	1.826E+007(Fitting)
400	1.078E–020(Expt.)	2.620E–009(Expt.)	3.743E+004(Expt.)	8.49	1.137E-010 (Expt.)	5.454E+006(Expt.)
	1.971E–020(Fitting)	2.619E–008(Fitting)	3.747E+004(Fitting)		1.137E–010(Fitting)	5.453E+006(Fitting)
450	1.000E–025 (Expt.)	2.039E–010(Expt.)	1.242E+006(Expt.)	2.76	3.819E–010(Expt.)	1.883E+005(Expt.)
	1.000E–025(Fitting)	2.040E–010(Fitting)	1.242E+006(Fitting)		3.818E–010(Fitting)	1.884E+005(Fitting)
500	5.626E–018(Expt.)	1.564E–010(Expt.)	2.721E+005(Expt.)	1.78	1.399E–009(Expt.)	1.058E+005(Expt.)
	7.298E–018(Fitting)	1.564E–010(Fitting)	2.721E+005(Fitting)		1.400E–009(Fitting)	1.058E+005(Fitting)

3.6 Modulus study

Smallest capacitance and also non-Debye type relaxation mechanism can be explained by modulus study of a material. Figure 5(a-b) express real modulus (M′) and imaginary modulus (M″) at some specific temperature range (25°C to 500°C) of this studied material. From these figures, it can be observed that the curves corresponding to M′ tends to a lower value (~zero) at the low-frequency region for all the respective temperatures while at higher frequency an asymptotic value is observed. Owing to the involvement of short-range mobile charge carriers, the nature of M′ almost attains a constant value at high frequency and hence reflects the conduction phenomenon in the material [48,49]. M″ modulus spectrum analysis has been carried out to identify the regions dominated by mobile short-range/ long-range charge carriers. Figure 5(b) displays the appearance of the peak which consistently appears to shift near to the higher frequency zone with increase in temperature. The formation of peaks confirm the presence of a relaxation phenomenon. The movement of peak maxima using a particular temperature towards the high-frequency side indicates the existence of a temperature-dependent relaxation mechanism in the fabricated BFMCO sample. Charge carriers are mobile over long range before the appearance of peak maxima while these are confined by potential wells and allowed to move in short range at the higher frequency zone [50,51]. Thus, the motions of charge carriers are changed from long to short range at the higher frequency zone. Figure 5(c) indicates the Cole-Cole plots at some specific temperature range of 25°C to 500°C and the semi-circular arcs appear in this plot confirms the semiconducting nature of this double perovskite. Two semicircular arcs in the Cole-Cole plot found in this sample demonstrated the grain and grain boundary contribution in overall impedance.

3.7 AC conductivity study

Figure 6(a) represents ac conductivity (σ_{ac}) versus frequency at different temperatures ranging from 25°C to 500°C. The conductivity data has been calculated by means of empirical relation: $\sigma_{ac} = \omega\varepsilon_r\varepsilon_0\tan\delta$, where the symbols represent their usual meaning. The plateau-type behavior of ac curves at low frequency for all the corresponding temperatures is ascribed to the long-range translational motion of ions representing the dc conductivity (σ_{dc}) [52].

Again, from the conductivity plot, it is observed that with the rise in temperature conductivity value increases which supports the negative temperature coefficient effect of resistance [53]. The presence of two different d-block cations (Fe^{2+} and Mn^{4+}) at the B-site in the prepared lead-free double perovskite contributes towards the migration of loosely bound ions which not only helps to the excitation of thermally activated charge carriers but also helps towards the smooth conduction mechanism [54]. Figure 6(b) represents ac conductivity (σac) against 1000/T at some specific frequency range of 1 kHz to 1 MHz. The lower part of the conductivity plots has been linearly fitted to calculate the activation energy using the Arrhenius Equation i.e., σdc = σ0 exp (-Ea/KBT), where the symbols represent its usual meaning. The calculated activation energies are 499.2 meV, 330 meV, 180.6 meV, 67.2 meV, 15.7 meV, 15.4 meV and 15.1 meV at 1kHz, 10 kHz, 100 kHz, 300 kHz, 500 kHz, 700 kHz and 1 MHz respectively. The obtained activation energy value supports that the electrical conduction mechanism is mostly dominated by the same type of charge carriers i.e., may be due to the involvement of thermally activated short-range charge carriers [55].

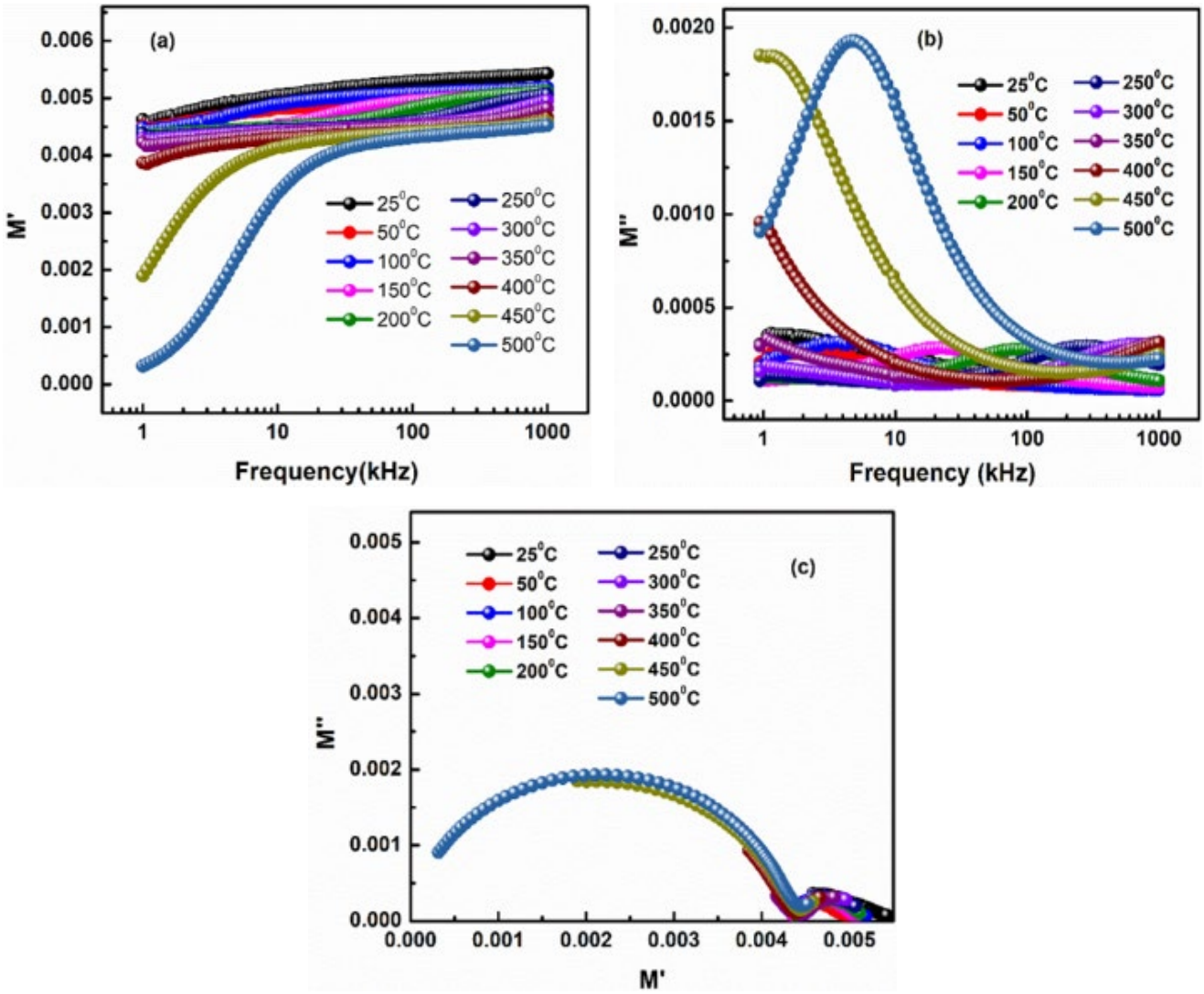

Figure 5. (a) Frequency vs. real modulus (M′), (b) Frequency vs. imaginary modulus (M″) and (c) Cole-Cole plots at specific temperatures of the BFMCO ceramic

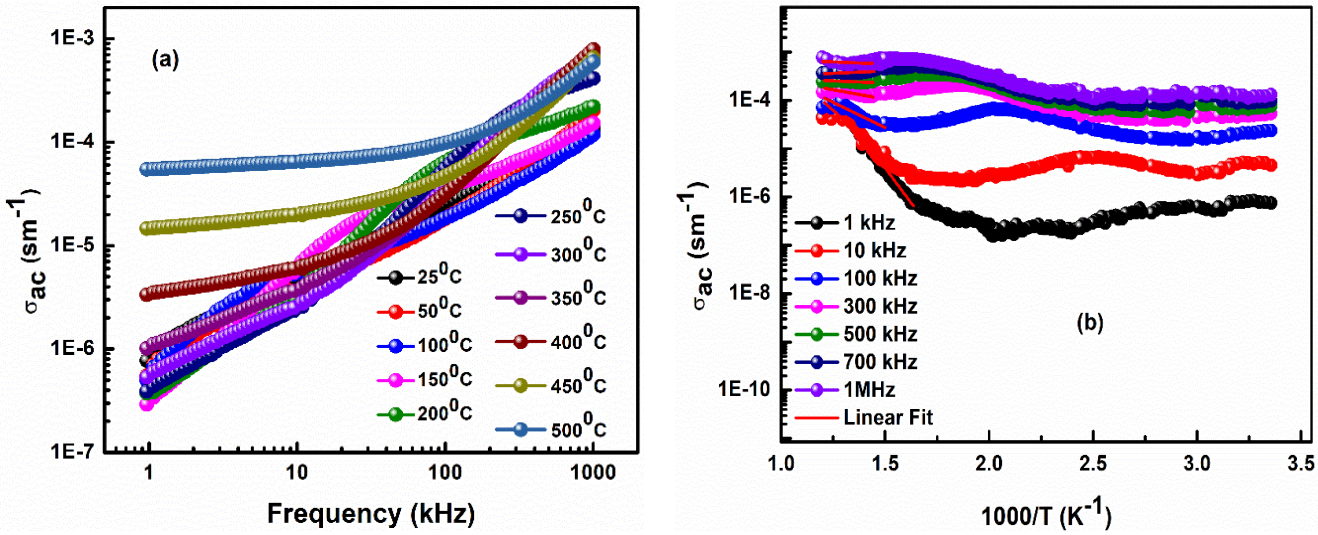

Figure 6. (a) ac conductivity against frequency and (b) ac conductivity against 1000/T of the BFMCO ceramic.

4. Conclusion

Multiferroic double perovskite composite material of $Bi_2FeMn_{0.94}Ce_{0.06}O_6$ was successfully synthesized through solid state reaction process having average crystallite size of 52.4 nm. XRD analysis indicates the crystalline and pure nature of the sample. The conductivity mechanism influenced by grains and grain boundaries were shown by the microstructural analysis. The elemental tracing of EDX spectra checked the existence of all constituent elements in the sample both atomic and weight percentages. Again, the colour mapping suggested the dispersal of all components (Bi, Fe, Mn, Ce, and O) across the entire surface of the material and supports the compositional purity. Maxwell-Wagner dielectric dispersions were observed in this material. Analysing the dielectric data against frequency and temperature yields a higher dielectric constant and lower tangent loss, suggesting that this material could be a promising choice for energy storing devices. Nyquist's plot and Cole-Cole's plot explained the NTCR behaviour which were claimed by the impedance versus frequency study and hence suggested that the prepared material may be used as a semiconductor. Both impedance and modulus study revealed the existence of non-Debye type of relaxation in this material. The presence of thermally stimulated conduction mechanism is observed in the material from AC conductivity studies.

Data availability statement

Data can be supplied on the request.

Conflict of Interest

Authors declare that they have no conflict of interest.

Acknowledgment

Authors would like to thank the host Institute for XRD and SEM-EDX characterization of our sample and there is no funding for this reported work.

References

[1] V. M. Teresita, A. Manikandan, B. A. Josephine, S. Sujatha, and S. A. Antony, "Electromagnetic properties and humidity-sensing studies of magnetically recoverable $LaMg_xFe_{1-x}O_{3-\delta}$ perovskite nano-photocatalysts by sol-gel route," *Journal of Superconductivity and Novel Magnetism*, vol. 29, no. 6, pp. 1691-1701, 2016.

[2] B. A. Josephine, A. Manikandan, V. M. Teresita, and S. A. Antony, "Fundamental study of $LaMg_xCr_{1-x}O_{3-\delta}$ perovskite nanophoto-catalysts: sol-gel synthesis, characterization and humidity sensing," *Korean Journal of Chemical Engineering*, vol. 33, no. 5, pp. 1590-1598, 2016.

[3] V. Umapathy, A. Manikandan, S. A. Antony, P. Ramu, and P. Neeraja, "Structure, morphology and opto-magnetic properties of Bi_2MoO_6 nano-photocatalyst synthesized by sol–gel method," *The Transactions of Nonferrous Metals Society of China* , vol. 25, pp. 3271-3278, 2015.

[4] A. Manikandan, S. A. Antony, R. Sridhar, S. Ramakrishna, and M. Bououdina, "Synthesis and characterization of $Fe_2(MoO_4)_3$ nano-photocatalyst by simple sol-gel method", *Journal of Nanoscience and Nanotechnology*, vol. 16, pp. 987-993, 2016.

[5] R. Ramesh, and N. A. Spaldin, "Multiferroics: progress and prospects in thin films" *Nature Materials*, vol. 6, pp. 21-29, 2007.

[6] T. Wang, L. Jin, C. Li, Q. Hu, and X. Wei, "Relaxor ferro-electric $BaTiO_3$–$Bi(Mg_{2/3}Nb_{1/3})O_3$ ceramics for energy storage application," *Journal of the American Ceramic Society*, vol. 98, p. 559, 2015.

[7] T. Wang, L. Jin, Y. Tian, L. Shu, Q. Hu, and X. Wei, "Micro-structure and ferroelectric properties of Nb_2O_5-modified $BiFeO_3$-$BaTiO_3$ lead-free ceramics for energy storage," *Materials Letters*, vol. 137, p. 79, 2014.

[8] K.-I. Kobayashi, T. Kimura, H. Sawada, K. Terakura, and Y. Tokura, "Room-temperature magnetoresistance in an oxide material with an ordered double-perovskite structure," *Nature*, vol. 395, pp. 677-680, 1998.

[9] S. Ravi, and C. Senthilkumar, "Multiferroism in new Bi_2FeMoO_6 material," *Materials Express* , vol. 5, 68-72, 2015.

[10] B. Zhao, L. Zhang, D. Zhen, S. Yoo, Y. Ding, D. Chen, Y. Chen, Q. Zhang, B. Doyle, X. Xiong, and M. Liu, "A tailored double perovskite nanofiber catalyst enables ultrafast oxygen evolution," *Nature Communincations*, vol. 8, p. 14586, 2017.

[11] Q. Tai, P. You, H. Sang, Z. Liu, C. Hu, H.L.W. Chan, and F. Yan, "Efficient and stable perovskite solar cells prepared in ambient air irrespective of the humidity," *Nature Communincations*, vol. 7, p. 11105, 2016.

[12] D.-L. Wang, H.-J. Cui, G.-J. Hou, Z.-G. Zhu, Q.-B. Yan, and G. Su, "Highly efficient light management for perovskite solar cells," *Scientific Reports* vol. 6, p. 18922, 2016.

[13] S. Ravi, and C. Senthilkumar, "Room temperature ferro-magnetism with high Curie temperature in La_2MnNiO_6 nano-particle," *Materials Letter*, vol. 164, pp. 124-126, 2016.

[14] S. Ravi, and C. Senthilkumar, "Low temperature ferro-magnetism in Bi_2MnMoO_6 double perovskite material," *Journal of Alloys and Compounds,* vol. 699, pp. 463-467, 2017.

[15] Y. Du, Z. X. Cheng, S. X. Dou, X. L. Wang, H. Y. Zhao, and H. Kimura, "Magnetic properties of Bi_2FeMnO_6: a multiferroic material with double-perovskite structure," *Applied Physics Letters*, vol. 97, p. 122502, 2010.

[16] L. Sun, Y.-W. Fang, J. He, Y. Zhang, R. Qi, Q. He, R. Huang, P. Xiang, X.-D. Tang, P. Yang, J. Chu, Y.-H. Chu, and C.-G. Duan, "The preparation, and structural and multiferroic properties of B-site ordered double-perovskite Bi_2FeMnO_6," *Journal of Materials Chemistry C*, vol. 5, pp. 5494-5500, 2017.

[17] Y. Du, Z. X. Cheng, S. X. Dou, X. L. Wang, H. Y. Zhao, and H. Kimura, "Magnetic properties of Bi_2FeMnO_6: a multiferroic material with double-perovskite structure," *Applied Physics Letters,* vol. 97, p. 122502, 2010.

[18] H. Zhao, H. Kimura, Z. Cheng, X. Wang, K. Ozawa, and T. Nishida, "Magnetic characterization of Bi_2FeMnO_6 film grown

on (100) $SrTiO_3$ substrate," *Physica status solidi (b),* vol. 4, pp. 314-315, 2010.

[19] X. Ou, Z. Li, F. Fan, H. Wang, and H. Wu, "Long-range magnetic interaction and frustration in double perovskites Sr_2NiIrO_6 and Sr_2ZnIrO_6," *Scientific Reports*, vol, 4, p. 7542, 2014.

[20] J. L Rosas, J. M Cervantes, J. Léon-Flores, E. Carvajal, J. A. Arenas, M. Romero, and R. Esca,illa, "DFT study on the electronic and magnetic properties of the Sr_2FeNbO_6 compound," *Materials Today Communications*, vol. 23, p. 100844, 2020.

[21] Y. Zhao, T. Liu, Q. Shi, Q. Yang, C. Li, D. Zhang, and C. Zhang, "Perovskite oxides $La_{0.4}Sr_{0.6}Co_xMn_{1-x}O_3$ (x = 0, 0.2, 0.4) as an effective electrocatalyst for lithium—air batteries," *Green Energy & Environment*, vol. 3, no. 1, 78-85, 2018.

[22] R. K. Parida, D. K. Pattanayak, B. Mohanty, B. N. Parida, and N. C. Nayak, "Dielectric and ferroelectric investigations of barium doped double perovskite Pb_2BiVO_6 for electronic and optical devices," *Materials Chemistry and Physics*, vol. 231, pp. 372-381, 2019.

[23] Y. Uratani, T. Shishidou, F. Ishii, and T. Oguch, "First-principles exploration of ferromagnetic and ferroelectric double-perovskite transition-metal oxides," *Physica B: Condensed Matter*, vol. 383, pp. 9-12, 2006.

[24] H-EM Musa Saad, and N. Rammeh, "Crystal, magnetic and electronic structures of 3d–5d ordered double perovskite Ba_2CoReO_6," *Solid State Communication*. vol. 248, pp. 129-133, 2016.

[25] S. E. Shirsath, S. S. Jadhav, B. G. Toksha, S. M. Patange, and K. M. Jadhav, "Influence of Ce^{4+} ions on the structural and magnetic properties of $NiFe_2O_4$," *Journal of Applied Physics,* vol. 110 p. 013914-1-8, 2011.

[26] M. Sahu, V. Vivekananthan, S. Hajra, D. K. Khatua, and S.-J. Kim, "Porosity modulated piezo-triboelectric hybridized nanogenerator for sensing small energy impacts," *Applied Materials Today*, vol. 22, p. 100900, 2021.

[27] N. Kumar, A. Shukla, N. Kumar, S. Hajra, S. Sahoo, and R. N. P. Choudhary, "Structural, bulk permittivity and impedance spectra of electronic material: $Bi(Fe_{0.5}La_{0.5})O_3$," *Journal of Materials Science: Materials in Electronics*, vol. 30, pp. 1919-1926, 2019.

[28] D. Bonardo, N. Darsono, S. Humaidi, A. Imaduddin and N. S. Silalah, "Effect of calcination frequency on the thermoelectric properties of Ti doped $CuCrO_2$ by solid state method," *Journal of Metals, Materials and Minerals*, vol. 33, 1785, 2023.

[29] S. Panda, S. Hajra, K. Mistewicz, P. In-na, M. Sahu, P. M. Rajaitha, and H. J. Kim, "Piezoelectric energy harvesting systems for biomedical applications," *Nano Energy*, vol. 100 p. 107514, 2022.

[30] V. M. Goldschmidt, "Die Gesetze Der Krystallochemie," *Naturwissenschaften*, vol. 14, pp. 477-485, 1926.

[31] R. D. Shannon and C. T. Prewitt, "effective ionic radii in oxides and fluorides," *Acta Crystallographica Section B*, vol. 25, pp. 925-946, 1969.

[32] R. D. Shannon, "Revised effective ionic radii and systematic studies of interatomic distances in halides and chalcogenides," *Acta Crystallographica Section A*, vol. 32, p. 1976.

[33] A. Corriero, C. Cuocci, C. Giacovazzo, A. Moliterni, R. Rizzi, N. Corriero, and A. Falcicchio, "EXPO2013: A kit of tools for phasing crystal structures from powder data," *Journal of Applied Crystallography*, vol. 46, pp, 1231-1235, 2013.

[34] E. Wu, "POWDMULT: An interactive powder diffraction data interpretation and indexing program, ver. 2.1, School of Physical Science, Flinders University, Australia, 1989.

[35] R. A. Young (Ed.), The Rietveld Method, Oxford University Press, Oxford, 1995.

[36] M. Ajmal, and A. Maqsood, "Influence of zinc substitution on structural and electrical properties of $Ni_{1-x}Zn_xFe_2O_4$ ferrites," *Meterials Science and Engineering: B*, vol. 139, pp. 164-170, 2007.

[37] D. Panda, S. S. Hota, and R. N. P. Choudhary, "Development of a novel triple perovskite barium bismuth molybdate material for thermistor-based applications," *Meterials Science and Engineering: B,* vol. 296, p. 116616, 2023.

[38] S. S.Ashima, R. A. Agarwal, and M. N. Ahlawat, "Structure refinement and dielectric relaxation of M-type Ba, Sr, Ba-Sr, and Ba-Pb hexaferrite," *Journal of Applied Physics,* vol. 112 pp. 14110-14115, 2012.

[39] C. G. Koops, "On the dispersion of resistivity and dielectric constant of some semiconductors at audio frequencies," Physical Review Journal, vol. 83, pp.121-124, 1951.

[40] S. K. Parida, and R. N. P. Choudhary, "Preparation method and cerium dopant effects on the properties of $BaMnO_3$ single perovskite," *Phase Transition,* vol. 93, pp. 981-991, 2020.

[41] K. Pradhan, D. S. Kumari, V. S. Puli, P. T. Das, D. K. Pradhan, A. K., J. F. Scott, and R. S. Katiyar, "Correlation of dielectric, electrical and magnetic properties near the magnetic phase transition temperature of cobalt zinc ferrite," *Physical Chemistry Chemical Physics,* vol. 19, pp. 210-216, 1017.

[42] S. Mishra, R. N. P. Choudhary and S. K. Parida, "Structural, dielectric, electrical and optical properties of Li/Fe modified barium tungstate double perovskite for electronic devices," *Ceramics International*, vol. 48, no. 12, pp. 17020-17033, 2022.

[43] P. Gogoi, P. Srinivas, P. Sharma, and D. Pamu, "Optical, dielectric characterization and impedance spectroscopy of Ni-substituted $MgTiO_3$ thin films," *Journal of Electronic Materials*, vol. 45 pp. 899-909, 2016.

[44] D .L. Rocco, A. A. Coelho, S. Gama, and M. de C. Santos, "Dependence of the magnetocaloric effect on the A-site ionic radius in isoelectronic manganites," *Journal of Applied Physics,* vol. 113, p. 113907, 2013.

[45] I. Coondoo, N. Panwar, A. Tomar, A. K. Jha, and S. K. Agarwal, "Impedance spectroscopy and conductivity studies in $SrBi_2(Ta_{1-x}W_x)_2O_9$ ferroelectric ceramics," *Physica B: Condensed Matter,* vol. 407, pp. 4712-4720, 2012.

[46] F. S. Moghadasi, V. Daadmehr, and M. Kashf, "Characterization and the frequency thermal response of electrical properties of Cu nano ferrite prepared by sol-gel method," *Journal of Magnetism and Magnetic Materials,* vol. 416, pp. 103-109, 2016.

[47] H. Saghrouni, S. Jomni, W. Belgacem, N. Hamdaoui, and L. Beji, "Physical and electrical characteristics of metal/ Dy_2O_3/ p-GaAs structure," *Physica B: Condensed Matter,* vol. 444, pp. 58-64, 2014.

[48] S. Thakur, R. Rai, I. Bdikin, and M. A. Valente, "Impedance and modulus spectroscopy characterization of Tb modified $Bi_{0.8}A_{0.1}Pb_{0.1}Fe_{0.9}Ti_{0.1}O_3$ ceramics," *Journal of Materials Research,* vol. 19, pp. 1-8, 2016.

[49] S. A. Jawad, A. S. Abu-Surrah, M. Maghrabi, and Z. Khattari, "Electric impedance study of elastic alternating propylene–carbon monoxide copolymer (PCO-200)," *Physica B: Condensed Matter,* vol. 406, pp. 2565-2569, 2011.

[50] P. G. R. Achary, R. N. P. Choudhary, and S. K. Parida, "Structure, electric and dielectric properties of $PbFe_{1/3}Ti_{1/3}W_{1/3}O_3$ single perovskite compound, process," *Applied Ceramics*, vol.14 pp. 146-153, 2020.

[51] M. Pollak, and T. H. Geballe, "Low-frequency conductivity due to hopping processes in silicon," *Physical Review*, vol. 122, pp. 1742-1753, 1961.

[52] J. R. Macdonald, "Comparison of the universal dynamic response power-law fitting model for conducting systems with superior alternative models," *Solid State Ionics*, vol. 133 pp. 79-97, 2000.

[53] F. A. Abdel-Wahab, H. M. Maksoud, and M. F. Kolkata, "Electrical conduction and dielectric relaxation in semiconductor SeSm0.005," *Journal of Physics D: Applied Physics*, vol. 39 pp. 190-195, 2006.

[54] A. Ghosh, S. Bhattacharya, D. P. Bhattacharya, and A. Ghosh, "Frequency-dependent conductivity of cadmium vanadate glassy semiconductor," *Journal of Physics: Condensed Matter*, vol. 20, pp. 35203-35205, 2008.

[55] S. Halder, S. Bhuyan, S. N. Das, S. Sahoo, R. N. P. Choudhary, and P. Das, "Structural, morphological, dielectric and impedance spectroscopy of lead-free Bi (Zn 2/3 Ta 1/ 3) O 3 electronic material," *Applied Physics A*, vol. 123, pp. 1-8, 2017.